Supplementary Material

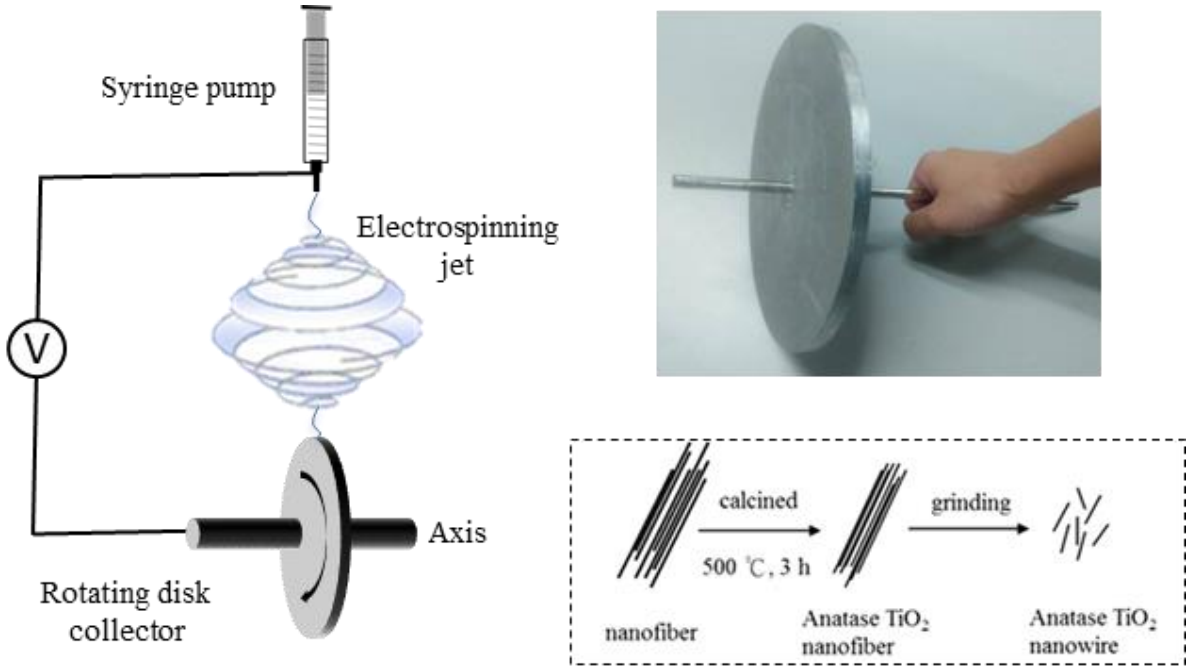

Figure S1. Electrospinning of TiO_2 nanofibers.

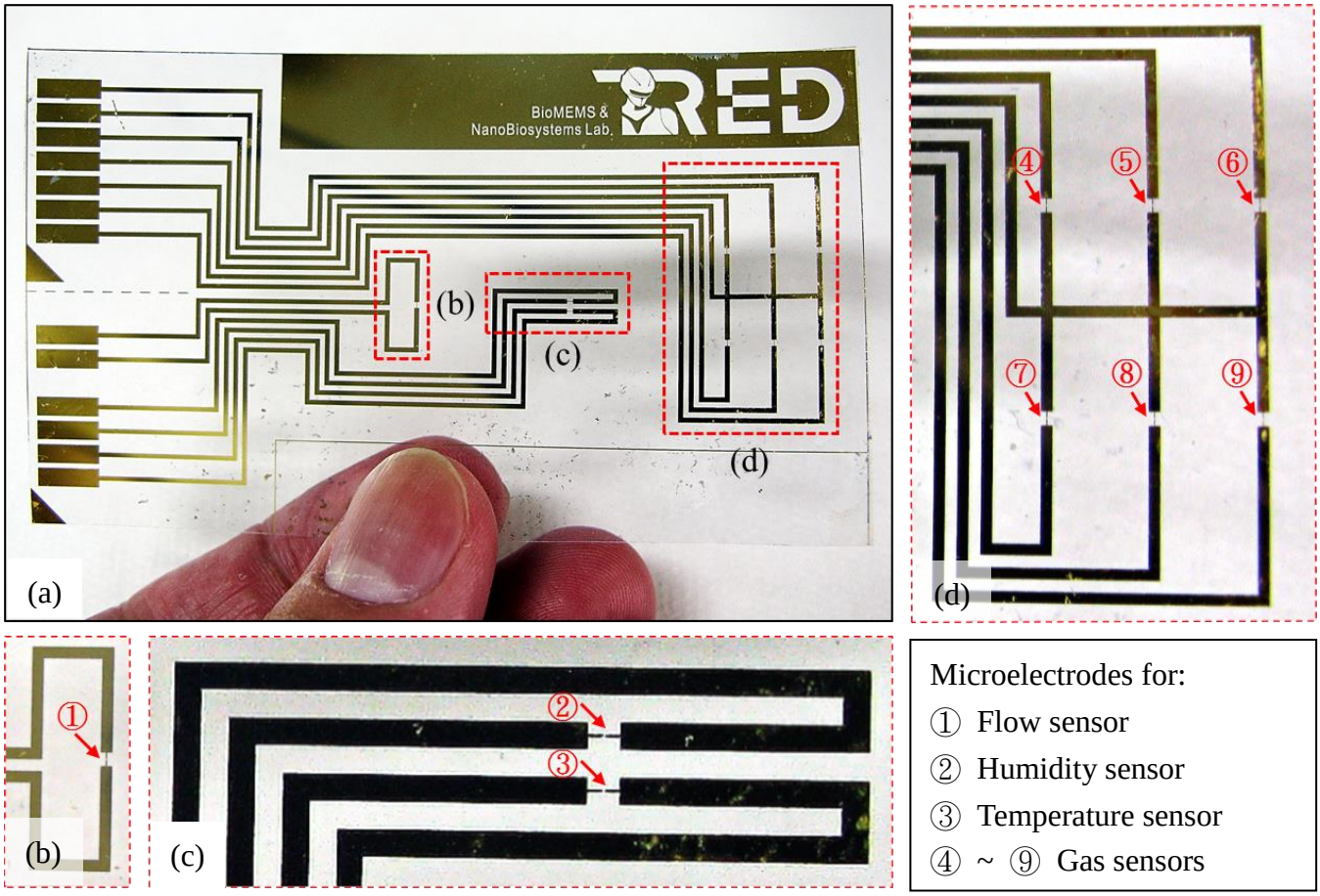

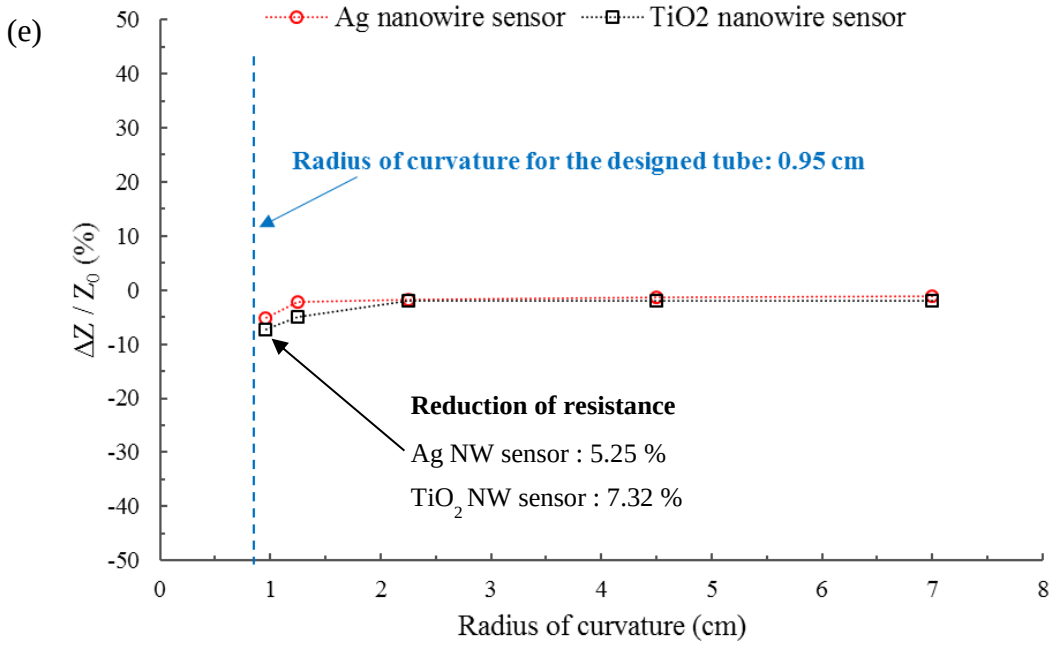

Figure S2. Images of the fabricated flexible electrodes array and impedance measurements of NW sensors. Optical images of the (a) electrode sensor array on a 125-μm-thick PET film, (b) microelectrode for flow sensor (highly magnified), (c) microelectrodes for temperature and humidity sensors, and (d) six microelectrode arrays for gas sensing (highly magnified). (e) Relative change in the impedance of the single Ag and TiO_2 NW sensors as a function of radius of curvature.

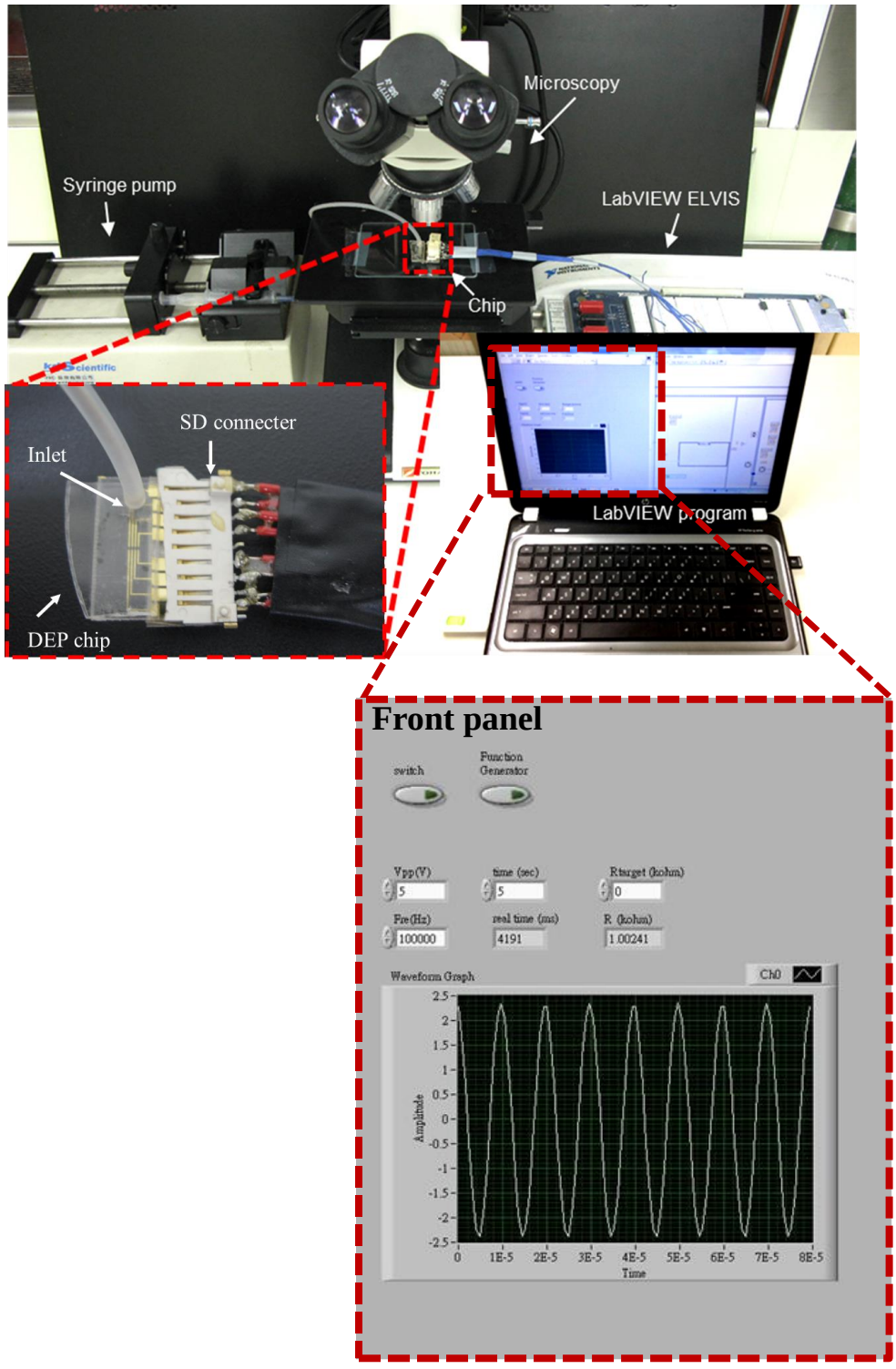

Figure S3. Experimental setup for dielectrophoretical assembly of the single-nanowire sensors.

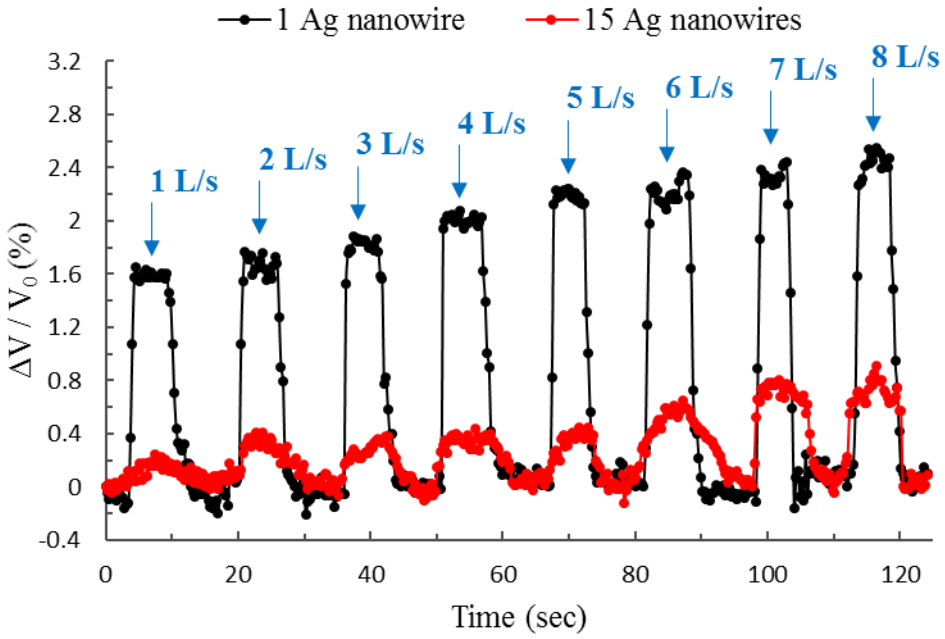

Figure S4. Comparison of the flow sensors based on single silver nanowire and multiple silver nanowires.

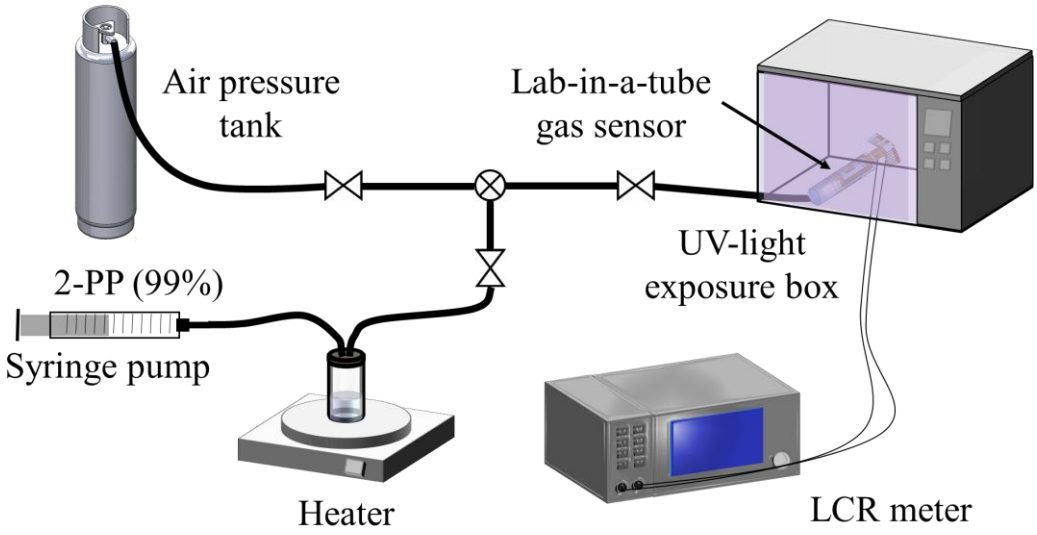

Figure S5. Experimental setup for characterization of the sensing tubes.

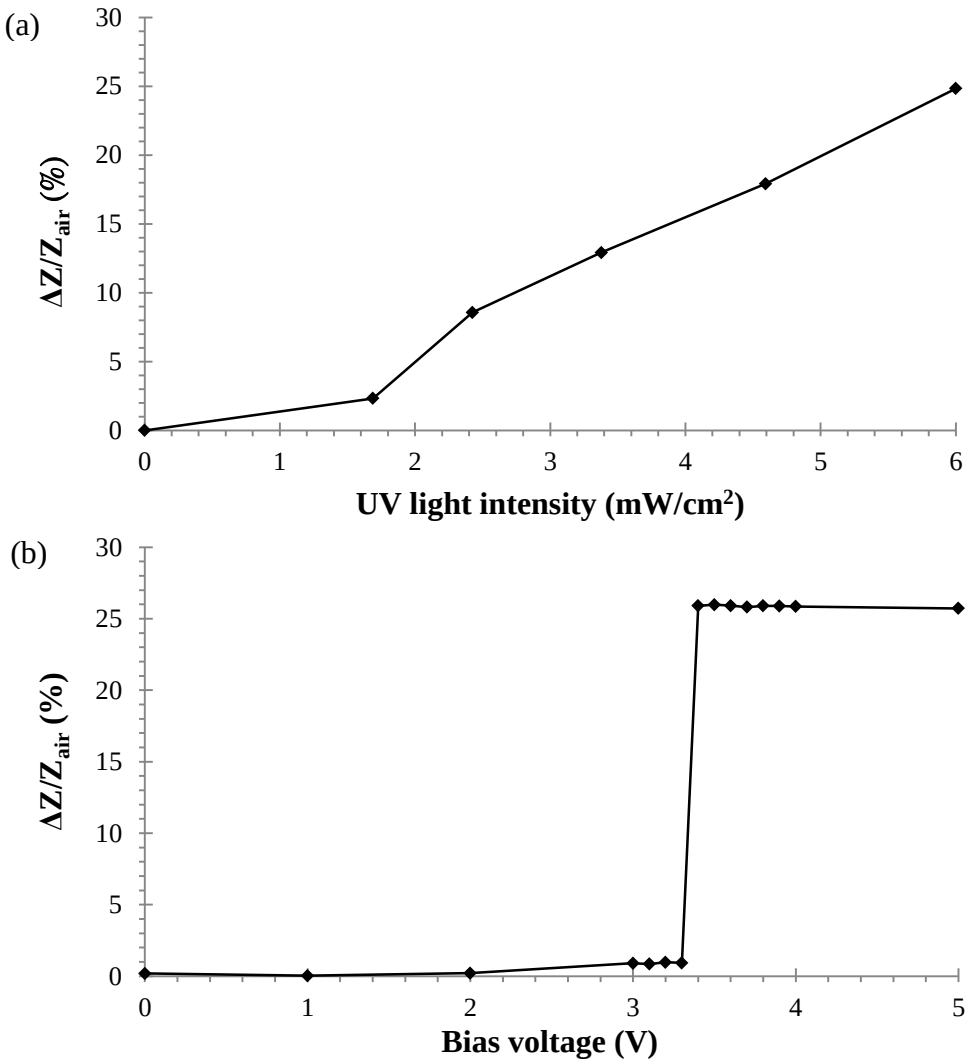

Figure S6. Characterization of the 2-PP sensors in microfluidic chips. (a) Response of the sensors under different UV light intensity and (b) response of the sensors under different bias voltages.

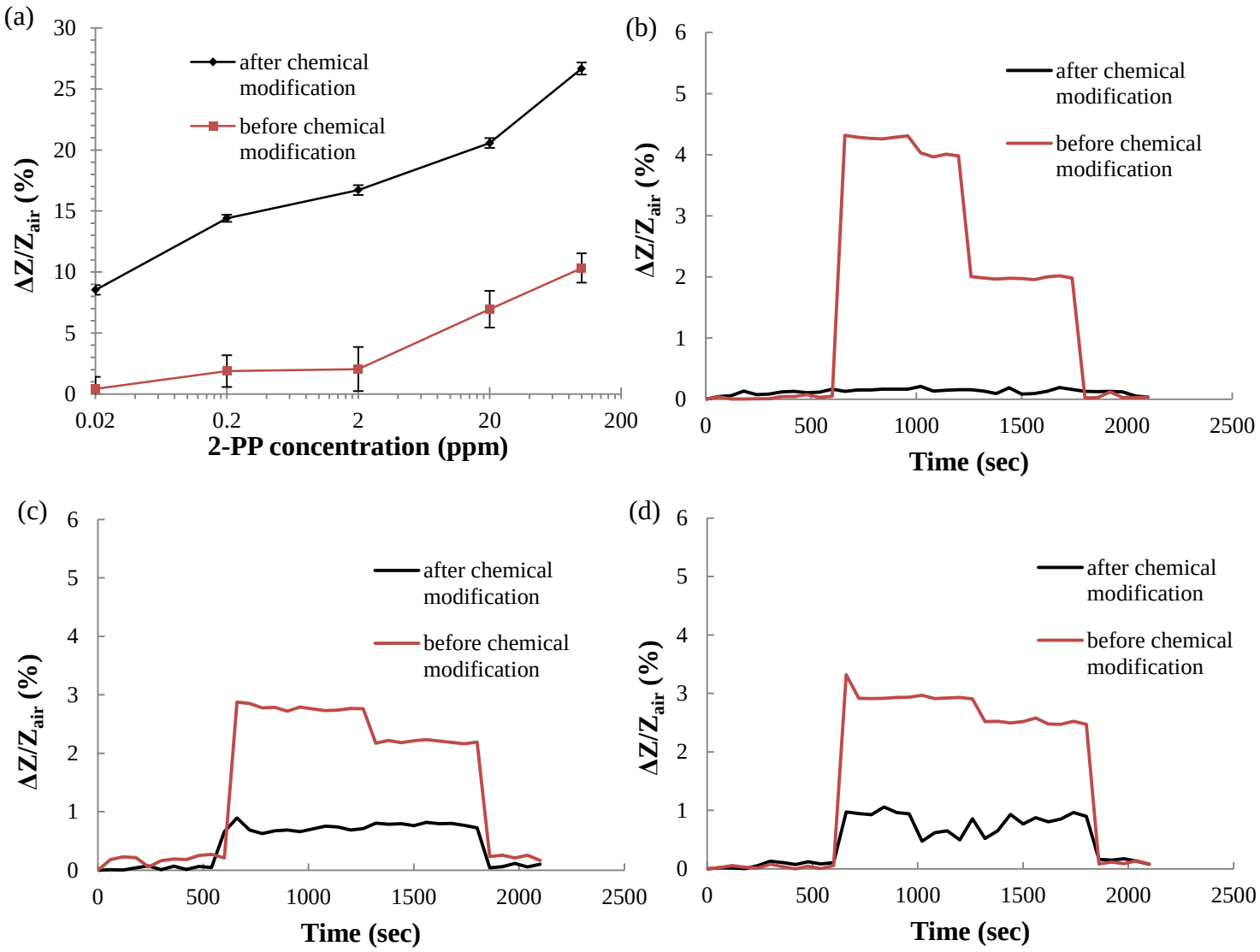

Figure S7. Characterization of the 2-PP sensors before/after APTMS modification in microfluidic chips. Comparison of the sensor response before/after APTMS modification (a) at different 2-PP concentrations, (b) at 200 ppb acetone, (c) at 200 ppb ethanol, and (d) at 200 ppb methanol.

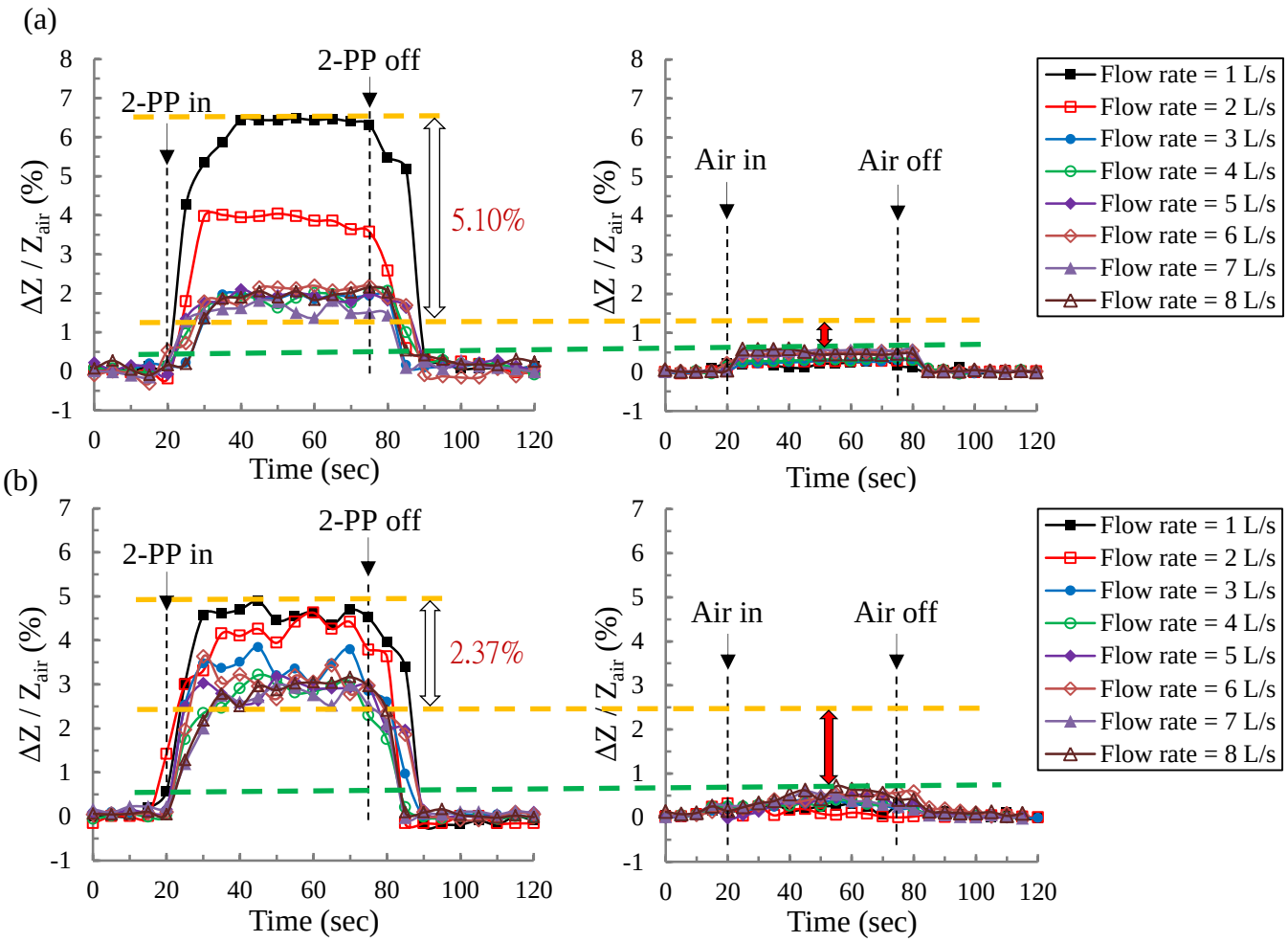

Figure S8. Comparison of the 2-PP detection at different flow rates with a concentration of 100 ppb for 5- and 30-cm long gas sensing tubes. (a) Dynamic response and recovery of the gas sensing with/without 2-PP at different flow rates in a 5-cm-long gas sensing tube and (b) dynamic response and recovery of the gas sensing with/without 2-PP at different flow rates in a 30-cm-long gas sensing tube.